Altering the allosteric pathway in IGPS suppresses millisecond motions and catalytic activity

George P. Lisi[a], Kyle W. East[a], Victor S. Batista[a], and J. Patrick Loria[a,b,1]

[a]Department of Chemistry, Yale University, New Haven, CT 06520; and [b]Department of Molecular Biophysics and Biochemistry, Yale University, New Haven, CT 06520

Edited by Peter E. Wright, The Scripps Research Institute, La Jolla, CA, and approved March 20, 2017 (received for review January 9, 2017)

Imidazole glycerol phosphate synthase (IGPS) is a V-type allosteric enzyme, meaning that its catalytic rate is critically dependent on activation by its allosteric ligand, *N*′-[(5′-phosphoribulosyl)formimino]-5-aminoimidazole-4-carboxamide ribonucleotide (PRFAR). The allosteric mechanism of IGPS is reliant on millisecond conformational motions for efficient catalysis. We engineered four mutants of IGPS designed to disrupt millisecond motions and allosteric coupling to identify regions that are critical to IGPS function. Multiple-quantum Carr–Purcell–Meiboom–Gill (CPMG) relaxation dispersion experiments and NMR chemical shift titrations reveal diminished enzyme flexibility and a reshaping of the allosteric connectivity in each mutant construct, respectively. The functional relevance of the observed motional quenching is confirmed by significant reductions in glutaminase kinetic activity and allosteric ligand binding affinity. This work presents relevant conclusions toward the control of protein allostery and design of unique allosteric sites for potential enzyme inhibitors with regulatory or therapeutic benefit.

allostery | NMR | community networks | millisecond motions

The underlying principles of allosteric regulation have been a focal point of enzymology and structural biology for decades as studies of allostery have evolved from two phenomenological models (1, 2) to recognize structural and conformational ensembles that define a broad range of enzymatic states (3–6). As a result, a great deal of emphasis has been placed on understanding dynamic contributions to allostery (7–12) and factors that enable small fluctuations in local conformations of enzymes to propagate information over large distances. A well-developed understanding of dynamic allostery opens up numerous avenues for insight into protein engineering (13, 14), drug design (15), and mechanistic biochemistry (16–22). To establish universal principles for relevant enzymes, however, a link between dynamics and function must be made.

The heterodimeric enzyme imidazole glycerol phosphate synthase (IGPS) plays a crucial role in amino acid and purine biosynthesis in bacteria and other microorganisms by sequentially catalyzing the hydrolysis of glutamine (Gln) in its HisH subunit and the cyclization of the substrate and allosteric effector *N*′-[(5′-phosphoribulosyl)formimino]-5-aminoimidazole-4-carboxamide ribonucleotide (PRFAR) in its HisF subunit (Scheme 1). IGPS is a V-type allosteric enzyme that is inactive unless PRFAR is bound, and communication between the active and effector sites is driven by the enhancement of conformational flexibility, namely, fluctuations taking place on the millisecond timescale (22–24). Based on NMR and computational evidence, these motions are believed to propagate from the PRFAR binding site to the glutaminase binding site, thereby disrupting a hydrogen bond between V51 and P10 of HisH. This H bond prevents formation of the oxyanion hole site necessary for glutamine hydrolysis, and its disruption allows IGPS to conformationally sample the activated state. Recently, we have advanced these studies and demonstrated that activation of IGPS is dependent on the ability of allosteric effectors to stimulate domain-wide motions in the HisF subunit and ligands that induce greater motion within the central $(\alpha\beta)_8$ barrel are more effective activators of glutaminase chemistry (22). NMR and computational community network studies proposed an optimal allosteric pathway through networks of HisF amino acid residues that link the PRFAR binding site and adjacent flexible loop 1 to residues comprising a central hydrophobic cluster essential for catalysis, as well as salt bridge residues at the dimer interface (25, 26). These previous results suggest important amino acids in each community that, upon mutation, should disrupt the IGPS allosteric network. The demonstrated importance of the networks suggests these mutations will alter the protein dynamics and that the resulting changes to the dynamical network will affect the corresponding functional properties of the enzyme.

The prior community network analysis showed that a feature of PRFAR binding is the strengthening of some communities at the expense of others, which involved multiple residues switching between communities. (25) In particular, there was an increase in communication between the HisF community, *f*3′, which contained secondary-structure elements *f*β1, *f*β2, *f*β3, *f*β4, *f*α2, *f*α2, and *h*α1, and community *h*2′, which encompassed the glutaminase active site and *h*P10 (*SI Appendix*, Fig. S1). This community connectivity is the most correlated route of communication between HisF and HisH. Throughout the manuscript, we distinguish HisF and HisH residues and communities with lowercase *f* and *h*, respectively. Additional community interactions in the PRFAR activated state occurred between community *f*3′ and *f*4′, which include residues from *f*β1, *f*β2, *f*α1, and loop 1. To examine the impact of perturbations to these allosteric communities and pathways, we engineered four IGPS variants (V12A, K19A, V48A, and D98A) that introduce an alanine residue at crucial positions within HisF (Fig. 1) but distant to the PRFAR binding site. The first residue, V12 in *f*β1, represents a residue from the apo community, *f*3 that switches to *f*1′ in the allosterically activated enzyme. In this PRFAR activated state, the *f*1′ community forms a weak network with the glutaminase community *h*2′. The second residue, K19, is located in loop 1, in the apo community *f*3, and switches to the *f*4′ community in the PRFAR-bound state. The third residue, V48, is located in

Significance

The enzyme imidazole glycerol phosphate synthase (IGPS) from *Thermotoga maritima* is a potential therapeutic target absent in mammals but present in bacteria, plants, and fungi. The reported findings on how to affect allosteric pathways and suppress catalytic activity are particularly relevant to establish and alter allosteric mechanisms that could represent targets for drug discovery. In particular, many plant and human pathogens that infect the immunocompromised patient have an IGPS that is highly homologous to the *Saccharomyces cerevisiae* and *T. maritima* enzymes. It has also been demonstrated that gene knockouts of IGPS subunit HisF can increase the susceptibility of bacteria to β-lactam antibiotics and lessen their infectivity.

Author contributions: G.P.L., V.S.B. and J.P.L. designed research; G.P.L. and K.W.E. performed research; G.P.L., K.W.E., V.S.B., and J.P.L. analyzed data; and G.P.L. and J.P.L. wrote the paper.

The authors declare no conflict of interest.

This article is a PNAS Direct Submission.

[1]To whom correspondence should be addressed. Email: patrick.loria@yale.edu.

This article contains supporting information online at www.pnas.org/lookup/suppl/doi:10.1073/pnas.1700448114/-/DCSupplemental.

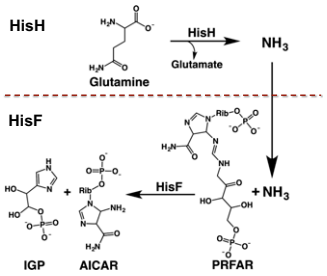

Scheme 1. Reaction catalyzed by *Thermotoga maritima* IGPS. The HisH subunit catalyzes Gln hydrolysis, and the HisF subunit catalyzes the cyclization of the allosteric activator PRFAR. Ammonia generated in the HisH reaction traverses the dimer interface (dashed line), where it is used as a substrate in the HisF reaction.

β-strand 2 in the hydrophobic cluster of the HisF α/β barrel. In the allosterically activated enzyme, V48 moves to the important *f*3′ community. Lastly, D98 is near the subunit interface in *f*β4 and is also involved in community *f*3′ when PRFAR is bound. Moreover, each of these residues is known to be flexible in WT IGPS in the fully activated ternary complex as probed by NMR and/or molecular-dynamics (MD) simulations. These residues are 10.2, 10.0, 7.5, and 18 Å, respectively from the PRFAR binding site.

With the established relationship between enzyme flexibility and allosteric communities in IGPS, we report a solution NMR investigation in which the millisecond timescale flexibility and enzyme function of these four single-point mutants is examined. These mutants behave similarly to WT IGPS in the apo state but are more rigid than the WT enzyme in substrate-mimicked ternary complexes. Interestingly, IGPS variants also show a range of diminished glutaminase kinetics and altered ligand-binding properties. We find that single-point mutations along the IGPS allosteric pathway are enough to suppress and reshape the dynamical connectivity within HisF and that this disruption is correlated to substantial losses in enzyme function, including the ability of the allosteric effector, PRFAR, to enhance glutaminase catalysis. These studies highlight the importance of protein-wide millisecond motions for catalytic activity in IGPS.

Results

Regions Affected by Ligand Binding Vary Across a Series of IGPS Mutants. Changes in the global structure of apo IGPS caused by replacement of V12, K19, V48, or D98 with alanine are minimal, as NMR spectral differences arise primarily near the site of mutation in both $^{1}H^{15}N$ heteronuclear single-quantum coherence (HSQC) and $^{1}H^{13}C$ heteronuclear multiple-quantum coherence (HMQC) NMR spectra (*SI Appendix*, Figs. S2 and S3). However, structural changes in these mutants in response to ligand binding to form acivicin- (a Gln mimic) and PRFAR-bound ternary complexes are more substantial and affect each IGPS variant differently. Changes in the environments of backbone amide resonances of IGPS were monitored in a series of $^{1}H^{15}N$ transverse relaxation optimized spectroscopy (TROSY) (27) HSQC NMR spectra with increasing concentrations of PRFAR (*SI Appendix*, Fig. S2). Combined chemical shift perturbations ($\Delta\delta_{^{1}H^{15}N}$) from these titrations are plotted for each IGPS ternary complex and mapped onto the HisF structure in Fig. 2.

The numbers of statistically significant PRFAR-induced shifts, determined from a 10% trimmed mean of the entire dataset, are greatly reduced in three IGPS variants, K19A, V48A, and D98A, which show only 13, 10, and 11 shifts above the cutoff, respectively. The V12A variant, however, displays 31 chemical shift perturbations above the significance cutoff, nearly the same as the 33 perturbations observed in WT IGPS, although the locations of shifts in each complex differ. Nonetheless, each ternary complex displays some degree of chemical shift perturbation due to PRFAR binding in locations spanning the entire HisF protein sequence, consistent with our previous findings of a widely dispersed allosteric network (22).

Decreased Spectral Broadening Suggests Rigidity in IGPS Mutants. Formation of the WT IGPS ternary complex (PRFAR plus the Gln analog acivicin) results in 67 amide resonances being broadened beyond detection (26% of HisF, Fig. 2 *A* and *B*).

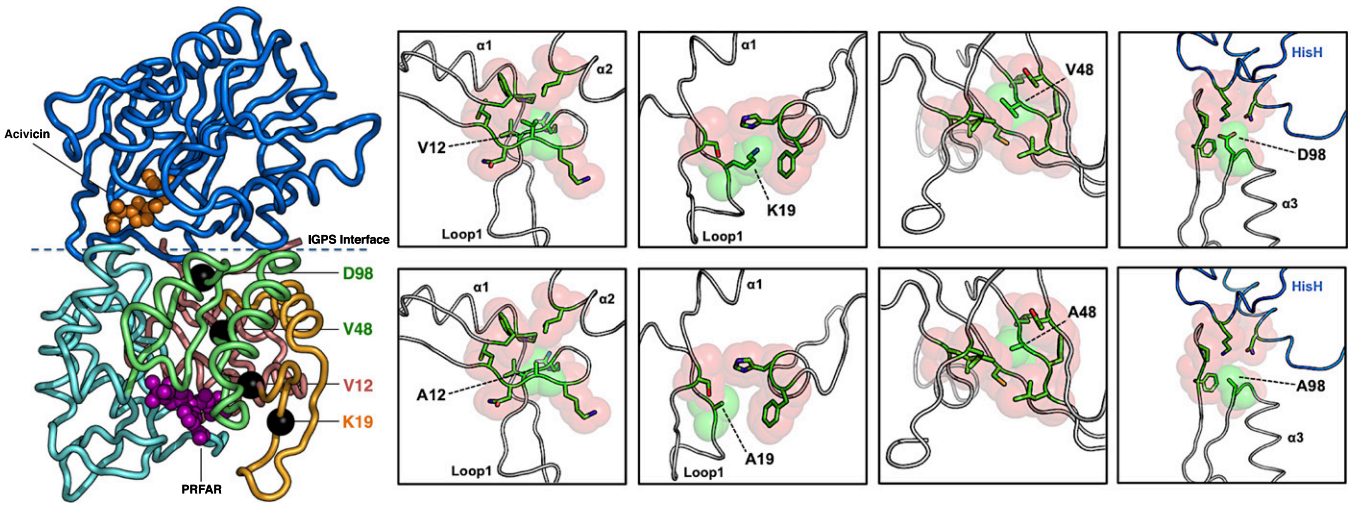

Fig. 1. Structure of *T. maritima* IGPS. (*Left*) The HisH subunit (blue) contains the glutaminase active site (the Gln analog acivicin is shown in orange spheres), and the HisF subunit binds the allosteric activator PRFAR (purple spheres). A well-defined noncovalent interface (blue dashed line) joins the two subunits. The HisF subunit is colored according to dynamic communities identified in a network analysis by Rivalta et al. (25), where communities *f*1′, *f*2′, *f*3′, and *f*4′ (symbolizing the PRFAR-bound enzymatic state) are colored light red, cyan, light green, and orange, respectively. Additional information on the contents of each community can be found in *SI Appendix*. Black spheres indicate selected mutation sites designed to alter the IGPS allosteric pathway. (*Right*) Close-up views of mutation sites showing the WT residue (top panels) and corresponding alanine mutations (bottom panels, generated with the Pymol mutagenesis function) (48). Alterations to structural packing are shown by van der Waals' contacts between residues within 5 Å of the terminal functional groups of V12, K19, V48, or D98. The site of mutation is highlighted in green spheres, whereas surrounding contacts are shown as pink spheres. Important structural elements are labeled in each panel.

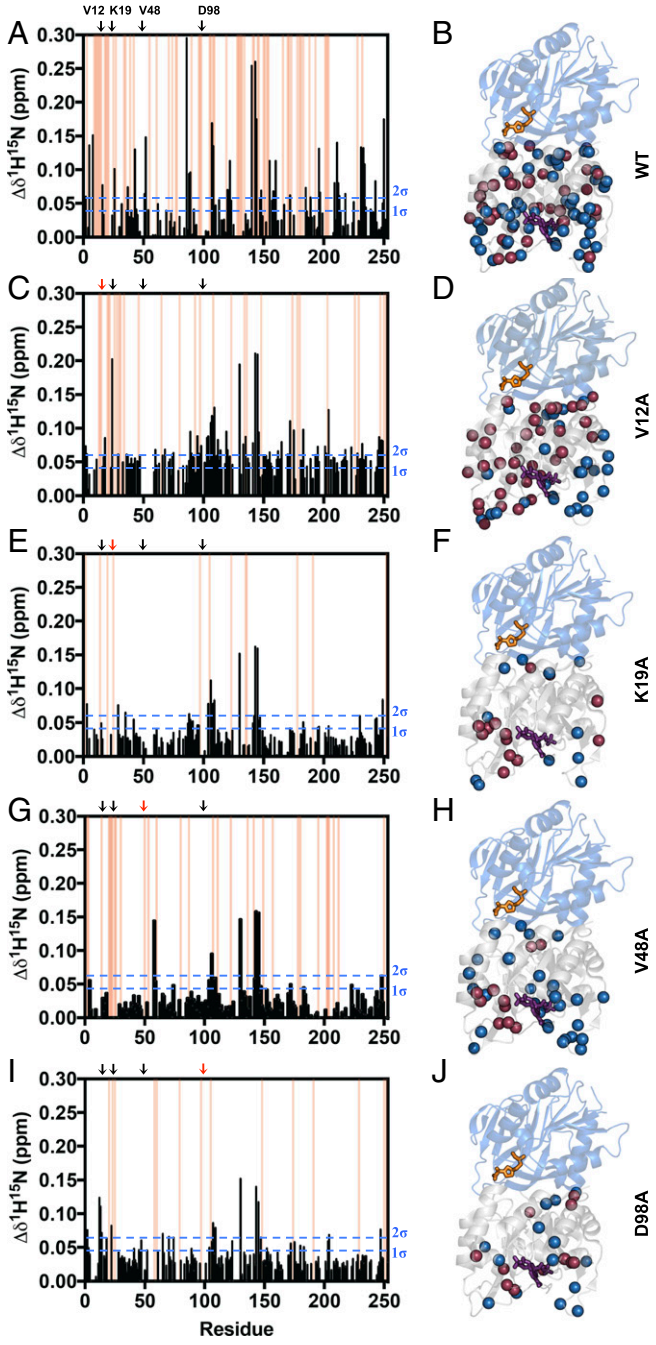

Fig. 2. Chemical shift perturbations caused by PRFAR binding. Combined chemical shift values taken from $^{1}H^{15}N$ HSQC spectral titrations of acivicin-bound IGPS with PRFAR are shown for (*A*) WT, (*C*) V12A, (*E*) K19A, (*G*) V48A, and (*I*) D98A. Shifts were determined by $\Delta\delta = \sqrt{(\Delta\delta_{HN}^2 + \Delta\delta_{NH}^2/25)/2}$ (49). Light pink vertical bars represent resonances that are broadened beyond detection during the course of each titration. Blue dashed lines indicate 1σ and 2σ above the 10% trimmed mean of all shifts. The red arrow above the corresponding panel indicates the location of each mutation. Shifts above the 2σ cutoff are mapped onto the HisF structures for the corresponding IGPS variants (*B*, *D*, *F*, *H*, and *J*) as red spheres. Blue spheres indicate amide resonances that are broadened beyond detection at saturating [PRFAR].

Coupled with significant chemical shift perturbations (22), areas of broadening comprising the effector (PRFAR) ligand site, loop 1, the hydrophobic cluster, and the HisF/HisH interface are prevalent, although nearly every structural element of HisF is affected. A similar degree of chemical shift perturbation is observed in the V12A IGPS ternary complex, but the number of exchange-broadened resonances (30 in V12A vs. 67 in WT) decreases significantly. The V12A ternary complex shows attenuated broadening of resonances near the IGPS dimer interface and hydrophobic cluster, but maintains similarly broadened features of the WT complex for residues at the bottom of the effector binding site and within loop 1, indicating that removal of V12 deviates from WT dynamical behavior at distant rather than local sites. A similar observation can be made for the V48A IGPS ternary complex, with almost all of the 31 broadened resonances corresponding to locations within loop 1 and the effector site, whereas the subunit interface and periphery of the hydrophobic cluster remain more static as demonstrated by narrow NMR resonances. Spectral broadening is most significantly attenuated in the K19A and D98A IGPS ternary complexes, which show only 12 and 14 broadened resonances, respectively. Both K19A and D98A IGPS show signs of increased rigidity in intersubunit residues as well as the PRFAR binding site and loop 1. This is particularly interesting in the case of the D98A variant because this residue is more than 15 Å away from the effector site, which provides further evidence that the IGPS allosteric pathway is highly sensitive to long-range perturbations. Taken together, NMR chemical shift perturbations and instances of exchange broadening in IGPS mutant ternary complexes reveal discontinuities in regions where the ternary WT IGPS is flexible (Fig. 2), particularly those connecting the effector site and dimer interface in K19A, V48A, and D98A IGPS. Although the effects observed for the HisF domain of V12A IGPS most closely resemble those of WT, reduced broadening leads to a more rigid structure and suggests that functional differences may be observed among these variants, as IGPS activity is known to be heavily reliant on flexibility of the HisF domain.

Altered Millisecond Motions in the Distal Mutants (Apo IGPS). Each IGPS mutant shows some evidence of millisecond timescale motions in both apo and ternary complexes, as summarized in *SI Appendix* (*SI Appendix*, Tables S1–S6). However, compared with the conformational flexibility previously reported for WT IGPS (24), the number and location of isoleucine, leucine, and valine (ILV) methyl groups with Carr–Purcell–Meiboom–Gill (CPMG) dispersion profiles is highly varied between the mutants. All mutations cause a reduction in the number of residues that experience millisecond motions in ternary complexes, and Fig. 3 presents representative CPMG relaxation dispersion curves for selected ILV residues in both apo and ternary IGPS. These side-chain methyl dynamics measurements showing reduced flexibility in the ternary mutant enzymes are consistent with the results seen from the reduction in amide resonance broadening.

Millisecond motions can be subdivided across four regions of IGPS: the active site (designated as all residues within 6 Å of PRFAR), the adjacent loop 1 (R16–D31), the hydrophobic L47–V48–F49–L50 cluster, and the dimer interface (all residues within 7 Å of HisH). In the apo enzyme as previously reported (22, 24), 17 ILV methyl groups exhibit dispersion in the WT enzyme. Of these 17 flexible methyl positions, 2 are found in the active site, 1 is found in loop 1, 2 in the hydrophobic cluster, and 3 more at the dimer interface, demonstrating that, even in its unliganded state, WT IGPS maintains a baseline level of plasticity in these critical allosteric regions. A binary complex of WT IGPS with the Gln mimic acivicin maintains indistinguishable dynamical features to those of the apo enzyme. Identical NMR experiments carried out on apo IGPS variants demonstrate very similar dynamic behavior among the enzyme family (Fig. 4*A*, *Top*). The V12A variant displays flexibility in three of the four allosteric regions in its apo state, but the overall number of flexible residues is 10 compared with 17 for WT. Mutation of K19, V48, or D98 allows IGPS to

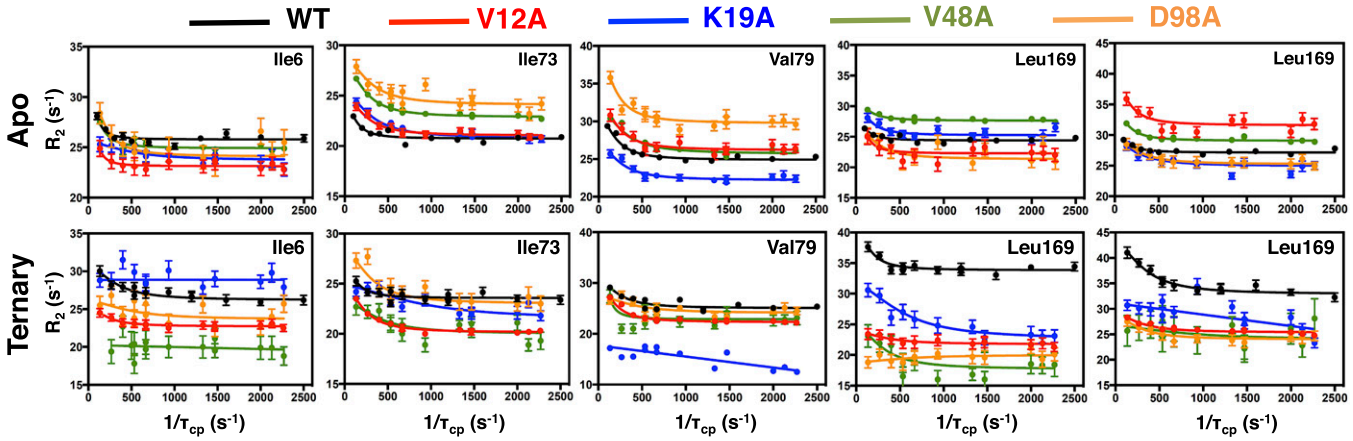

Fig. 3. Representative ^{13}C-MQ CPMG relaxation dispersion curves of WT (black), V12A (red), K19A (blue), V48A (green), and D98A (orange) IGPS. The top panels correspond to selected methyl groups in each apo enzyme, whereas the bottom panel displays curves from acivicin- and PRFAR-bound ternary complexes. Errors were determined from duplicate experiments.

retain the same number of flexible residues as that of apo WT, with small variations in location.

Altered Millisecond Motions in the Distal Mutants (Ternary IGPS). Formation of a WT ternary complex with acivicin and the allosteric effector PRFAR induces flexibility in 35 methyl groups including five active site residues, two residues in loop 1, three of the four hydrophobic cluster residues, and eight interfacial residues, as well as in other regions of the enzyme, highlighting the differences between apo and the fully activated ternary complex.

The V12A ternary complex is flexible at the active site, hydrophobic cluster, and dimer interface, and most closely recapitulates the dynamics of WT IGPS. However, the number of flexible residues in the V12A ternary complex is reduced by ~30%. K19A IGPS shows evidence of millisecond motions primarily at the dimer interface and other distant regions throughout HisF, although only 11 methyls appear flexible in total, a 70% reduction in the number of flexible residues compared with WT. The V48A variant shows no dynamic activation at the HisF/HisH interface in ternary complexes, and only a small cluster of residues along the allosteric pathway, near the effector binding site, exhibits millisecond motions, consistent with rigidity observed in the K19A complex. Ternary complexes containing the D98A mutation have one-half as many flexible residues undergoing millisecond motions

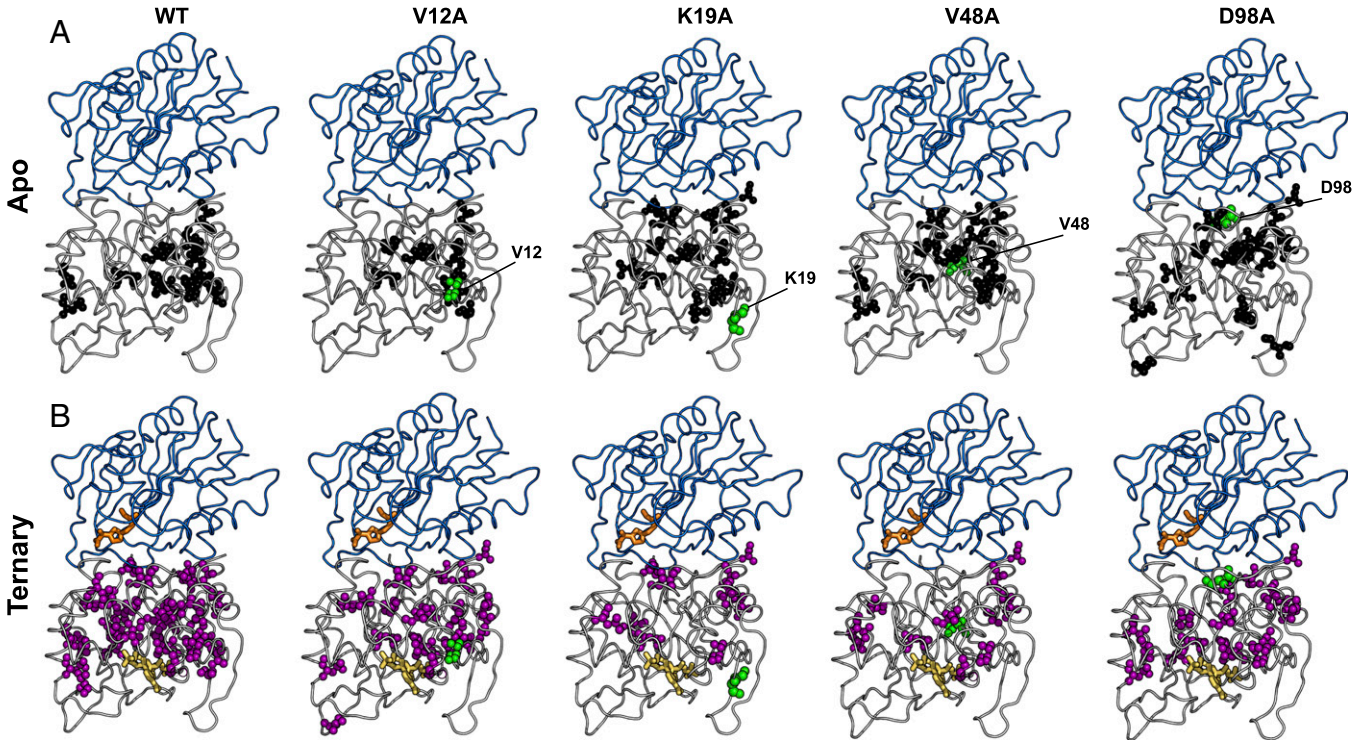

Fig. 4. Flexible residues determined from millisecond timescale relaxation dispersion experiments. Dynamic ILV residues in (*A*) apo (black spheres) and (*B*) ternary (purple spheres) WT IGPS and IGPS variants are mapped onto the structures of the HisF domain. Acivicin and PRFAR are shown in ternary complexes as orange and yellow sticks, respectively. The location of each mutation is shown in green spheres.

compared with those in WT IGPS. Moreover, only 8 of the remaining 20 flexible methyl groups within D98A IGPS occur in regions comprising the optimal allosteric pathway.

Clustering of k_{ex} Values Reveals a Loss of Concerted Motion in IGPS Ternary Complexes. Analyses of CPMG dispersion curves generated for apo IGPS enzymes reveal high degrees of similarity with WT in domain flexibility and the rate at which conformational states interconvert (*SI Appendix*, Fig. S4). Exchange rates (k_{ex}) of apo IGPS mutants are primarily clustered between 300 and 1,000 s^{-1} for various ILV residues, consistent with those of the apo WT enzyme. However, in the PRFAR-bound ternary complexes, significant differences exist between the WT and mutant enzymes. Millisecond conformational flexibility is assumed to be a concerted process in the substrate-mimicked ternary complex of WT IGPS because fits of CPMG relaxation dispersion data yield a global k_{ex} value of 225 ± 30 s^{-1} involving nearly 40 residues distributed throughout HisF (24). Statistical analyses of independent and global-fitting models of dynamic residues in mutant ternary complexes were found to favor concerted motion only in the V12A enzyme, whereas motions in K19A, V48A, and D98A IGPS were more appropriately described by independent

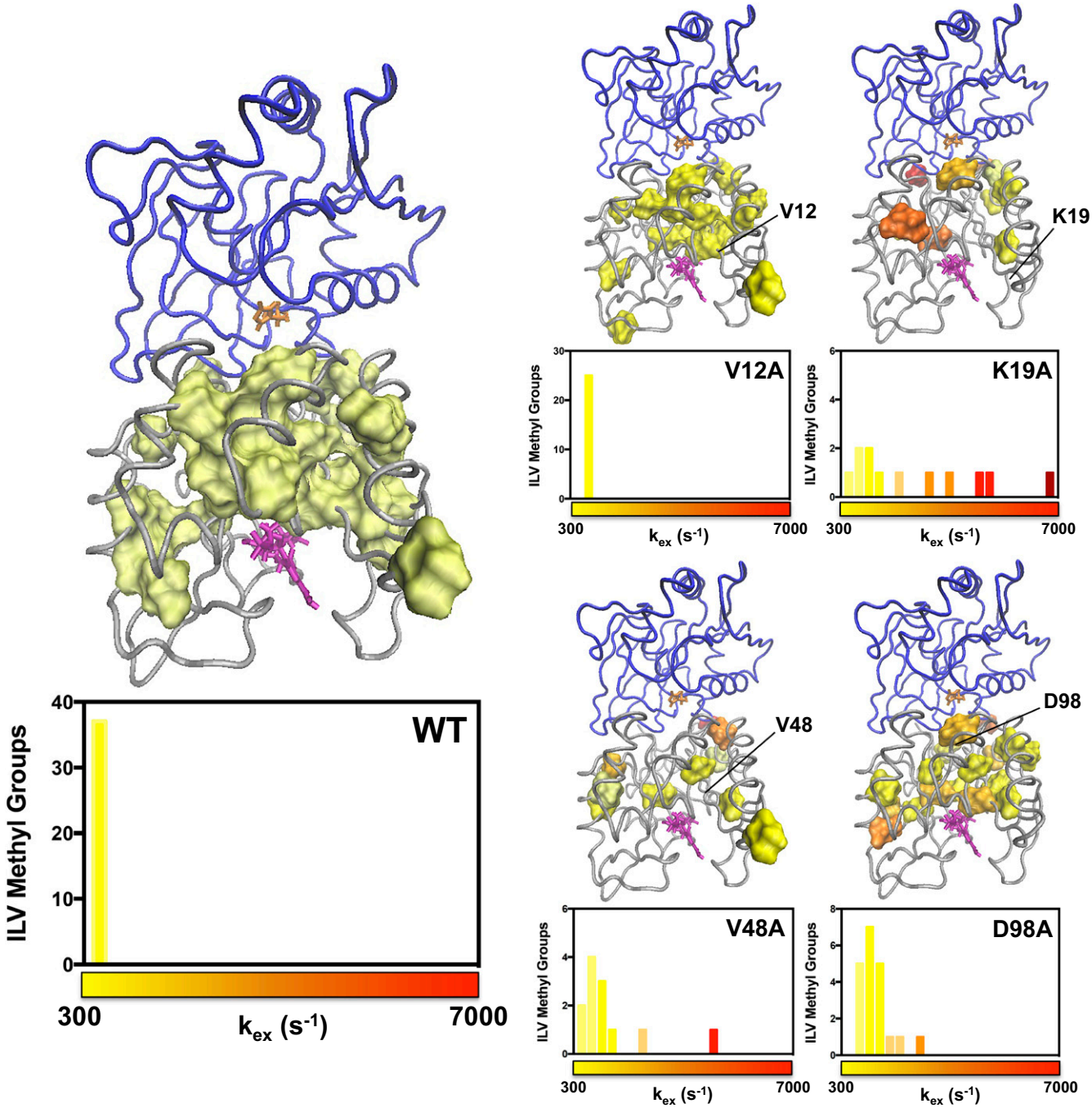

Fig. 5. Clustering of k_{ex} values determined from CPMG relaxation dispersion for IGPS ternary complexes. The distribution of k_{ex} is shown for each IGPS ternary complex, and the magnitudes of these distributions are mapped onto the HisF structure with identical color schemes. Bin sizing for data cutoffs was determined using a protocol outlined by Scott (50). PRFAR and acivicin are shown in purple and orange sticks, respectively.

Table 1. Kinetic parameters determined from glutaminase assays

	Activated*			Basal			
Enzyme	k_{cat}, s^{-1}	K_M, Gln, mM	k_{cat}/K_M, $M^{-1}s^{-1}$	k_{cat}, s^{-1}	K_M, Gln, mM	k_{cat}/K_M, $M^{-1}s^{-1}$	$\frac{k_{cat}/K_{M(activator)}}{k_{cat}/K_{M(basal)}}$
WT	3.62 ± 0.10	1.74 ± 0.22	2.08×10^3	1.65 (0.03) $\times 10^{-3}$	3.57 ± 0.76	4.60×10^{-1}	4,521
V12A	1.88 ± 0.05	1.40 ± 0.19	1.34×10^3	1.73 (0.03) $\times 10^{-3}$	4.12 ± 0.75	4.20×10^{-1}	3,095
K19A	0.57 ± 0.04	3.41 ± 0.42	1.66×10^2	5.40 (0.05) $\times 10^{-3}$	3.00 ± 0.88	1.80	92
V48A	0.24 ± 0.01	1.99 ± 0.43	1.22×10^2	3.28 (0.07) $\times 10^{-3}$	3.76 ± 0.51	8.72×10^{-1}	139
D98A	0.18 ± 0.02	3.11 ± 0.73	5.79×10^1	3.11 (0.03) $\times 10^{-3}$	2.88 ± 1.22	1.07	54

Michaelis–Menten parameters were determined from assays carried out in the presence (activator) and absence (basal) of saturating PRFAR.
*[PRFAR] was 1 mM (WT) and 11.5 mM (V12A, K19A, V48A, and D98A).

fits based on the Akaike information criterion (28). Fig. 5 highlights regions of concerted, albeit diminished millisecond motion in the V12A ternary complex. Flexibility is maintained at the effector site, hydrophobic cluster, and dimer interface with a global exchange rate of 433 ± 96 s^{-1}, about twofold faster than that of WT. Ternary complexes of K19A and V48A IGPS show clusters of even faster motion at the HisF/HisH interface and loop 1, respectively. Interestingly, D98A IGPS displays the narrowest distribution of k_{ex} among variants with uncorrelated motion and the greatest similarity in average exchange rate and dynamic coverage to that of WT or V12A. However, instances of uncorrelated exchange occur at the active site and motions are generally localized in areas outside of key structural elements. Distributions of k_{ex} values mapped onto the HisF domain of the IGPS structure demonstrates that contiguous pathways of similarly paced motions are scarce in three IGPS variants, consistent with a reshuffling of the allosteric communication pathway.

Altered IGPS Catalytic Activity in Dynamically Impaired Mutants. Prior NMR and computational work demonstrated a correlation between ligand-enhancement of millisecond motions and enzymatic activity (22, 25, 29). Therefore, kinetic assays that monitor glutamine hydrolysis were used to gain insight into the effects of mutation of critical residues in the IGPS allosteric pathway. In WT IGPS, PRFAR binding activates glutamine hydrolysis 5,000-fold over a nearly negligible basal rate in its absence. Kinetic parameters determined from glutaminase assays are reported for all IGPS enzymes in Table 1. Introduction of alanine at any of the chosen positions does not disrupt basal activity, although the mutations cause substantial kinetic impairments in the PRFAR-activated enzymes (Fig. 6), most notably in the K19A, V48A, and D98A constructs. The observation that k_{cat} and K_m for the basal glutamine hydrolysis reaction for the mutants are the same as WT indicates that the glutamine active-site integrity is maintained in the mutant IGPS enzymes. Thus, mutant IGPS catalytic activity is only altered due to its compromised ability to signal the glutaminase site to indicate that PRFAR is bound and to subsequently generate the motions needed for activation.

K19A and V48A show similar reductions in catalytic efficiency for the PRFAR-activated glutaminase reaction, which is an order

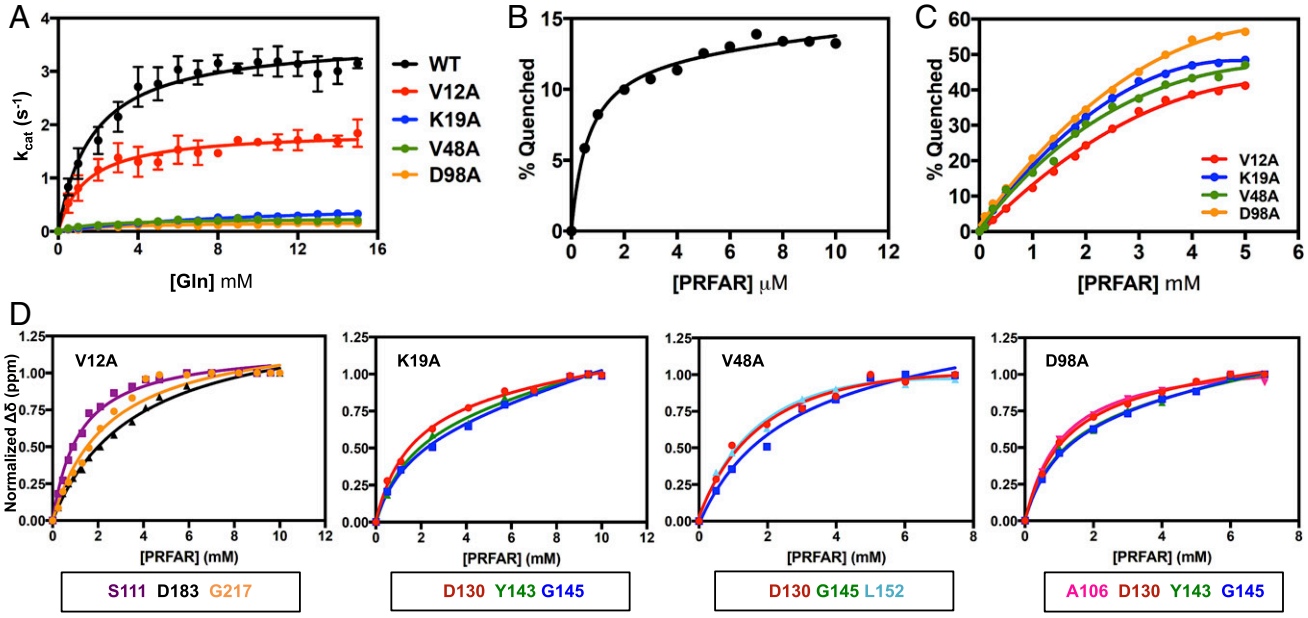

Fig. 6. Altered function of WT IGPS by alanine mutations. (*A*) Glutamine-dependent kinetic profiles of IGPS complexes in the presence of saturating PRFAR. Traces were fit for Michaelis–Menten kinetic parameters, which are reported in Table 1. Error bars are based on triplicate measurements and in some cases are smaller than the size of the data point. (*B* and *C*) Percentage of intrinsic Trp fluorescence intensity quenched in WT (*B*) and mutant (*C*) IGPS (λ_{max} = 328 nm). (*D*) Selected HisF resonances showing substantial chemical shifts during PRFAR ligand titrations (*SI Appendix*, Fig. S1). Representative data were normalized to the maximum chemical shift difference and fit to the equation $\Delta\delta = [(\Delta\delta_{max} + [PRFAR])/(K_D + [PRFAR])]$, where $\Delta\delta$ is the measured chemical shift, $\Delta\delta_{max}$ is the maximum saturated shift, [PRFAR] is the ligand concentration, and K_D is the ligand dissociation constant (51). Apparent ligand-binding affinities were determined from a global fit of all data for each IGPS sample. Residues used in the NMR titration fitting are given in boxes below each panel.

of magnitude below that measured for the WT enzyme, whereas the D98A variant is over 30-fold less active than WT. Interestingly, despite very similar chemical shift behavior between the two, K19A IGPS is approximately threefold more active than D98A, consistent with earlier work by Davisson, Wilmanns, and coworkers (30, 31) on the K19A and D98A enzymes, respectively. V12A is the only mutation that retains WT-like glutaminase activity with a k_{cat} value that is 50% that of WT IGPS, resulting in a similar reduction in catalytic efficiency. Interestingly, the V12A variant is also the only mutant that maintains global conformational motions in CPMG experiments and behaves most similarly to WT IGPS in ligand-binding titrations, reaffirming the connection between flexibility of the HisF domain and IGPS catalytic rate enhancement.

The overall similarity of (basal) glutaminase parameters among the five enzymes in the absence of PRFAR suggests that debilitating mutations truly affect allosteric information transfer that is essential to catalysis. Thus, differences in the ratios of catalytic efficiencies of the PRFAR-bound and apo enzymes reflect the extent of activation due to the effector ligand (Table 1). These data show that glutaminase activity in WT IGPS is stimulated >4,500-fold in the presence of PRFAR, which is in good agreement with the initial report of 4,900-fold activation by Davisson and coworkers (30). Introduction of single-point mutations in HisF has dramatic effects on PRFAR-induced activation of IGPS, as the V12A mutation reduces glutaminase activity to 70% that of WT, whereas the K19A, V48A, and D98A variants are reduced to ∼3% activity.

The observed decrease in catalytic activities for IGPS variants is also linked to a significant decrease in PRFAR binding affinity (Fig. 6). Fits of several NMR resonances during titrations of IGPS with PRFAR yield K_D values ∼1–2 mM, three orders of magnitude weaker than the measured affinity of WT IGPS. Because these mutations were introduced at positions that are distant from the effector binding site, such a reduction in PRFAR affinity suggests that small perturbations to the allosteric pathway are enough to impair proper function of the entire HisF domain. The altered function of IGPS mutants is further corroborated through quenching experiments that monitor the intrinsic fluorescence of two tryptophan residues as PRFAR is titrated into IGPS. Nearly 15% of the emission intensity of WT IGPS is quenched by PRFAR (Fig. 6 and *SI Appendix*, Fig. S5), presumably due to a slightly altered conformation of the tryptophan fluorophores upon saturation. A marked difference is observed in similar experiments with IGPS mutants, as the degree of fluorescence quenching ranges from 40 to 60%. Interestingly, the extent of quenching correlates inversely with the extent of glutaminase activity and allosteric coupling reported in Table 1, suggesting that these data may be a useful marker for predicting the impact of point mutations on IGPS activity.

Discussion

The stimulation of millisecond motions throughout the HisF subunit of IGPS is a critical component of efficient allosteric information transfer, and thus activation of glutamine hydrolysis. The degree of NMR line broadening in $^{1}H^{15}N$ HSQC spectra of WT IGPS along with the well-dispersed coverage of flexible ILV methyl groups among HisF structural elements demonstrate a domain-wide participation in dynamic allosteric signal propagation. Two previous works using a series of chemically related allosteric activators (22) and a community network analysis (25) provided the rationale for evaluating the effect of perturbations along the IGPS allosteric pathway. This work showed that ligands that enhance flexibility in the largest number of residues result in greater glutaminase activity. The community network analysis provided information on the dynamical connectivity among structural elements within HisF that allows propagation of the ligand-induced flexibility, which is essential for glutaminase activity. We selected allosteric nodes identified in those two studies as critical for the transduction of information across the IGPS interface.

We find that introduction of alanine residues at four node locations within HisF does not significantly perturb the global structure of the enzyme; however, chemical shift behavior during titrations with the allosteric activator PRFAR is varied among the WT and mutant enzymes, indicating that mutations affect the local environment and these perturbations are propagated along unique pathways throughout the HisF domain. An associated 500-fold decrease in PRFAR binding affinity is also observed. Furthermore, we find that NMR line broadening is greatly reduced in $^{1}H^{15}N$ HSQC spectra of IGPS mutants compared with that of WT, indicative of more rigid HisF in the mutant enzymes.

CPMG relaxation dispersion experiments probing millisecond motions in WT IGPS demonstrated a concerted, domain-wide participation in conformational exchange (22, 24). Similar concerted motions were observed in the ternary complex of the most catalytically active V12A variant, but attempts to fit dispersion curves of the remaining IGPS variants to a global exchange

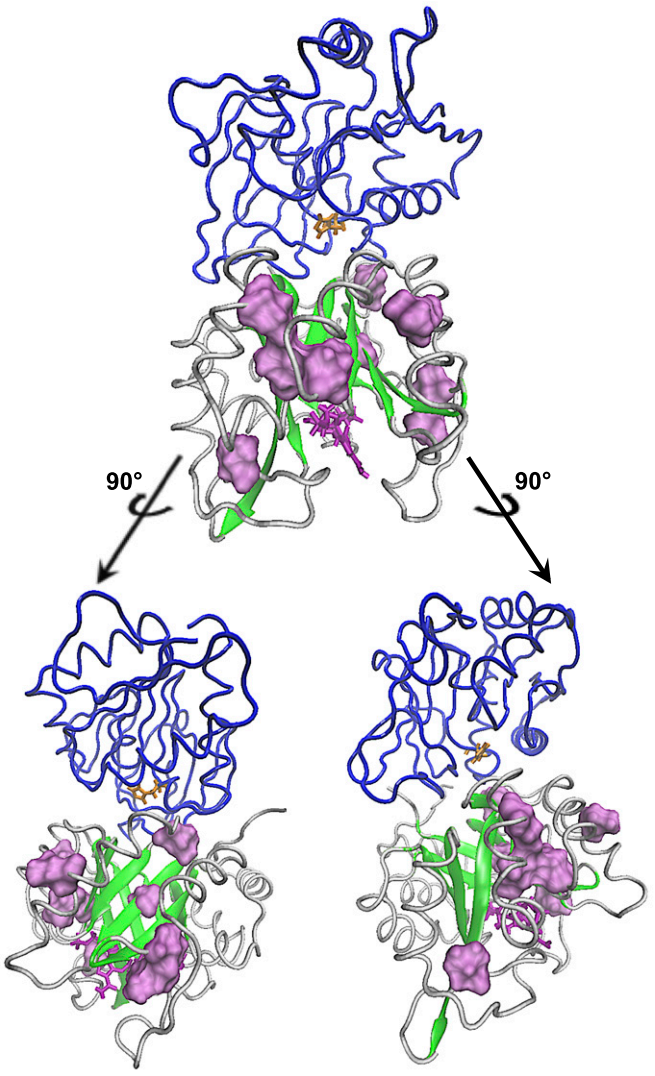

Fig. 7. Regions of millisecond motion unique to ternary WT IGPS. Flexible regions of HisF observed in the ternary complex of WT IGPS that are absent from V12A, K19A, V48A, or D98A ternary complexes are depicted as a purple surface. Many of these residues are located in portions of the central β-barrel (green).

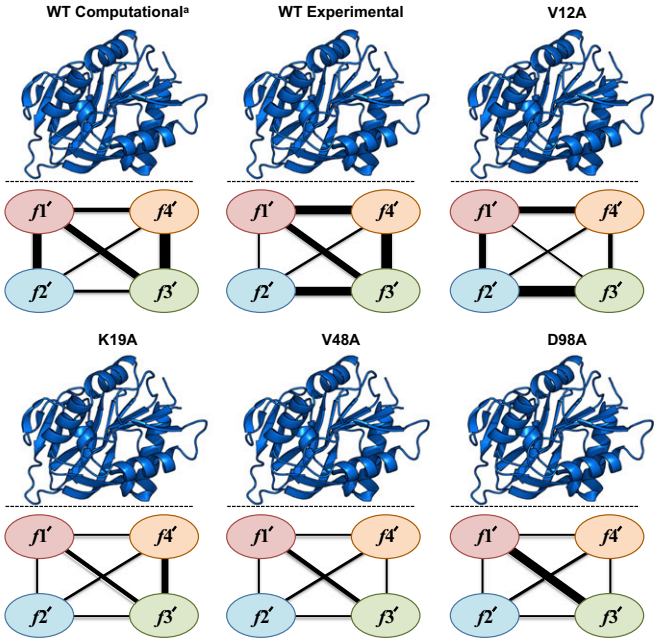

Fig. 8. Residues exchanging between dynamic communities in HisF upon PRFAR binding to IGPS. Community nomenclature reflects those described by Rivalta et al. (25) during computational analysis, serving as a basis for hypothesizing an experimental outcome. The "WT Computational" panel depicts residues that exchange dynamic communities during computational studies of PRFAR binding to HisF. [a]Reported and summarized in ref. 25. The "WT Experimental," "V12A," "K19A," "V48A," and "D98A" panels report exchange between dynamic communities for residues with significant chemical-shift perturbations caused by PRFAR binding to WT IGPS in NMR experiments. The same information is reported for each of the mutant enzymes. The thickness of the lines between each of the four HisF communities reflects a normalized measure of the number of residues exchanging between connected communities, where thicker lines indicate that a greater number of residues move between two connected communities during PRFAR binding to apo IGPS. A table containing all of the residues considered in these diagrams is provided in *SI Appendix*. The HisH subunit is shown in ribbon representation and the dashed line represents the IGPS dimer interface.

process were consistently less optimal compared with the analyses of individual methyl groups, indicating that perturbations of these sites disrupt concerted motions in the enzyme. Veglia and coworkers (21) recently reported a similar observation in studies of the ubiquitous signaling enzyme protein kinase A (PKA). The synchronous millisecond motions that regulate the open-to-close transition of the PKA binding cleft were disrupted by a single-point mutation, Y204A, in a residue that never interacts with the enzymatic substrate. The Y204A mutation in PKA was shown to redistribute conformational flexibility to noncritical areas of the enzyme and has no effect on faster (picosecond to nanosecond) motions. Moreover, work by the same group showed that a single amino acid deletion in the PKA substrate phospholamban resulted in the inability of this substrate to shift the conformation of PKA to the fully catalytically committed state. PKA also experienced attenuated motions when bound to the altered substrate compared with its natural phospholamban substrate (32). Similar behavior is also observed in the enzyme thimydylate synthase, where Lee and coworker (33) observed that a single C146S mutation significantly weakened substrate affinity and led to widespread chemical shift perturbations in the apo and substrate-bound enzyme, results that mirror the behavior we observed in IGPS variants.

A summary of the flexible residues that are unique to the WT IGPS ternary complex are shown in Fig. 7. This figure highlights critical flexible residues (V17, V18, V48, L63, I75, I83, I102, and I116) that remain rigid in all of the mutant enzymes. All of these residues are located in apo community *f*2 or *f*3 and switch to either *f*3′ or *f*4′ in the PRFAR-activated state. As noted previously, the *f*4′ and *f*3′ communities are essential for relaying the PRFAR signal to the active site (community *h*2′) of HisH. The prior network analysis showed that most correlated communities are between *h*2′ and *f*3′ in the PRFAR-bound state and that this was critical for communication with the Ω-loop in the HisH active-site region (25). To investigate how the mutants studied in this work altered the community networks, we generated experimentally derived networks based on NMR chemical shift and CPMG relaxation dispersion analysis and compared them to the community behavior previously identified by computational methods (Fig. 8 and *SI Appendix*, Fig. S6) (25). In these figures, we depict the communities in the PRFAR-activated state identified by Rivalta et al. (25) and show the number of residues that switch between that community from the apo state as the thickness of the line connecting the communities. We then compare our experimental data for the WT and four mutant enzymes to the computational results. Fig. 8 shows this community exchange for residues with PRFAR-induced chemical shift perturbations above the 2σ cutoff determined from Fig. 2 (indicating these residues experience a significant change in time-averaged chemical shift). To validate this approach, a comparison of WT experimental and computational communities (Fig. 8 *A* and *B*) indicate good reproduction of the computational results by the experiments. Data for the other mutants show deviations from the WT behavior particularly in residues that move into community *f*4′. Interestingly, V12A, the most active mutant (Fig. 8*C*) is most similar to WT, suggesting the importance of communities *f*4′ and *f*3′ and hinting at an origin for its retention of WT-like properties. We performed a similar analysis using the CPMG dispersion data in which the connecting line thickness represents flexible residues that undergo a change in dynamic community upon PRFAR binding (*SI Appendix*, Fig. S6). Like the chemical shift analysis, the WT experimental and computational community connections are similar and again V12A most resembles WT. A list of all residues used for this analysis and their apo and PRFAR-bound communities is provided in *SI Appendix*, Tables S7 and S8. In summary, the computational network analysis and NMR studies helped identify important allosteric communities and residues in IGPS. Mutation of these residues alters the interaction between the communities by disrupting the underlying millisecond motions and subsequently alters IGPS function.

We propose a reaction scheme that is consistent with the NMR, computational, and biochemical data to summarize these effects (Scheme 2).

The K_d values for PRFAR and glutamine were determined by isothermal titration calorimetry (24). These values are similar to their K_m values, and thus K_m likely represents the equilibrium binding of these ligands. The PRFAR-induced millisecond motions are depicted within the dashed box and depict the motions necessary to allow sampling of the active HisH conformer(s) indicated by the red color and asterisk. Glutamine hydrolysis and steps associated with it are likely rate-determining occurring at ~5 s^{-1}. Dissociation of the product glutamate occurs around 250 s^{-1} as determined by NMR line shape analysis. Based on this, the rate of the reaction depends on the concentration of E*-P-Gln, which is generated by the millisecond motions induced by PRFAR binding. We propose

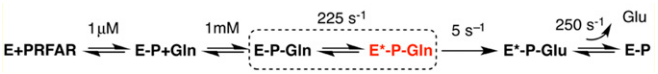

Scheme 2.

that mutation of critical network residues compromises the ability of IGPS to sample E*-P-Gln and thus results in lower catalytic activity. Thus, the ability of IGPS to form WT-like *f*3′ and *f*4′ communities is essential to this process. Whether the observed concerted motions are necessary for efficient sampling of the active conformer or whether they are simply a result of having an intact allosteric network is not known.

These data clearly highlight a link between altered dynamics of the HisF subunit and altered chemistry of the IGPS enzyme. Single amino acid substitutions, none of which are in the glutaminase subunit, have profound functional effects from distances of up to 25 Å. Moreover, this work demonstrates the utility of NMR as a method for probing dynamic regulatory pathways in enzymes. Our initial NMR characterizations of the IGPS bienzyme (22, 24), coupled with detailed molecular-dynamics simulations (25), predicted these sites as flexible allosteric hot spots that had potential to be exploited to modify communication between the HisF and HisH binding sites. Our results have strong implications for the rational design and control of protein allostery through the identification and subsequent alteration of conserved dynamic pathways.

Experimental Procedures

Materials. Antibiotics used in protein expression and other analytical grade chemicals were purchased from AmericanBio. 3-Acetylpyridine adenine dinucleotide (APAD) and glutamate dehydrogenase (GDH) used in kinetic assays were purchased from Santa Cruz Biotechnology and Affymetrix, respectively. PRFAR was synthesized as previously described (24).

Site-Directed Mutagenesis, Protein Expression, and NMR Sample Preparation. DNA containing HisF and HisH were cloned into pET43.1b vectors and transformed into BL21(DE3) cells in a manner described elsewhere (24). The HisH sequence contained a C-terminal histidine affinity tag. Plasmids containing the V12A, K19A, V48A, and D98A variants of HisF were constructed using a QuikChange Kit (Agilent Technologies) and designed primers synthesized by the W. M. Keck Oligonucleotide Synthesis Facility at Yale University School of Medicine. Insertion of the correct mutation was also verified at the W. M. Keck DNA Sequencing Laboratory at Yale University. Isotopically enriched HisF (^{2}H, ^{13}C, ^{15}N) and HisH (^{2}H) subunits were expressed at 37 °C in M9 minimal medium containing $CaCl_2$, $MgSO_4$, and MEM vitamins. Small cultures of HisF and HisH were grown overnight in LB medium. The following morning, the cloudy suspensions were used to inoculate a second set of LB cultures containing 50% D_2O, which were grown for 8–10 h and then used to inoculate a final set of LB cultures made with 95% D_2O. After 12 h of incubation, these cells were collected by centrifugation and resuspended in the final M9 growth medium. HisF was grown in 1.5 L of deuterated M9 with $^{15}NH_4Cl$ (Cambridge Isotope Labs) as the sole nitrogen source. Isotopic labeling of HisF Ile, Leu, and Val methyl groups was achieved by adding 60 mg/L α-ketobutyric acid [methyl-^{13}C; 3,3-D_2] and 100 mg/L α-ketoisovaleric acid [3-methyl-^{13}C; 3,4,4,4-D_4] (Cambridge Isotope Labs) 30 min before induction (34, 35). HisH was grown in 1 L of deuterated M9 supplemented with naturally abundant nitrogen and carbon isotopes. Cultures of HisF and HisH were grown to an OD_{600} of 0.8–1.0 before induction with 1 mM isopropyl β-D-1-thiogalactopyranoside.

HisF and HisH cell pellets were harvested after 7 h and resuspended in a buffer containing 10 mM Tris, 10 mM *N*-cyclohexyl-3-aminopropanesulfonic acid (CAPS), 300 mM NaCl, and 1 mM β-mercaptoethanol at pH 7.5. The suspensions were mixed together, and the cells were lysed by ultrasonication. Cell debris was removed by centrifugation. The resulting supernatant was applied to a Ni-NTA agarose column equilibrated with a buffer containing 10 mM Tris, 10 mM CAPS, 300 mM NaCl, and 1 mM β-mercaptoethanol at pH 7.5 The column was washed with ∼100 mL of the same buffer containing 15 mM imidazole at pH 9.5. The IGPS complex was eluted with the same buffer containing 250 mM imidazole at pH 9.5 and dialyzed extensively against a buffer containing 10 mM Hepes, 10 mM KCl, and 0.5 mM EDTA at pH 7.3. Following dialysis, the sample was washed and concentrated in an identical buffer containing 5% D_2O in an Amicon centrifugal cell (EMD Millipore).

Covalent modification of IGPS with the nonhydrolyzable Gln analog acivicin was achieved by incubating IGPS with two molar equivalents of acivicin for 8–10 h (22, 24, 36). Successful conjugation of IGPS was confirmed by a reduction in free thiol content with a DTNB assay. Excess acivicin was removed by dialysis against a buffer containing 10 mM Hepes, 10 mM KCl, 0.5 mM EDTA, and 5% D_2O at pH 7.3.

Ligand Titrations. NMR titrations were performed on a Varian Inova 600-MHz NMR spectrometer at 30 °C by collecting a series of ^{1}H-^{15}N TROSY HSQC spectra with increasing ligand concentration. The ^{1}H and ^{15}N carrier frequencies were set to the water resonance and 120 ppm, respectively. Samples of acivicin-conjugated WT, V12A, K19A, V48A, and D98A IGPS were titrated with PRFAR until no further perturbations were detected, to final ligand concentrations of 0.9, 10, 10, 7.5, and 6.9 mM, respectively.

Methyl-TROSY Multiple-Quantum CPMG Dispersion Experiments. Multiple-Quantum (MQ) CPMG experiments probing ILV methyl groups ($^{13}CH_3$) were performed on Varian Inova 600-MHz and Agilent 800-MHz NMR spectrometers at 30 °C, as previously described (37, 38). A constant relaxation delay period of 0.03 s was used in the CPMG pulse sequence, with a τ_{cp} array of 0.0, 0.4412, 0.46875, 0.50, 0.68182, 0.75, 1.07143, 1.5, 1.875, 2.5, 3.75, and 7.5 ms and 2.0-s recycle delay.

Spectral Processing and Data Analysis. NMR spectra were processed with NMRPipe (39) and analyzed in SPARKY (40). Transverse relaxation rates (R_2) were determined from peak intensities of each ILV methyl resonance at multiple τ_{cp} delay points with a Perl-based exponential curve-fitting script. Relaxation dispersion curves obtained at two static magnetic fields were generated by plotting R_2 vs. $1/\tau_{cp}$ using GraphPad Prism 7.0 (GraphPad Software) and fit simultaneously using the fast-limit CPMG equation, where uncertainty values were obtained from replicate spectra. Dual field relaxation dispersion data were also processed with RELAX (41–43) using the R2eff, NoRex, and MMQCR72 (two-site Carver–Richards) models (44). Relax was used to globally fit residues undergoing dispersion in V12A, K19A, V48A, and D98A IGPS, and statistical analyses of independent and global models indicated that only V12A IGPS was well-described by a global dynamic process based on the Akaike information criterion (28, 45, 46). Dynamic residues in all other IGPS variants were treated independently. In doing this, we make the assumption that groups of amino acid residues with the same k_{ex} value are moving in a concerted fashion. This is probably the simplest explanation of the data but may not be the case. It could be possible that the residues coincidentally have the same exchange rate constant but are not moving in a concerted fashion.

Glutaminase Kinetic Assays. Glutaminase activity of IGPS in the presence of PRFAR was measured as previously described (29), after adaptation from the procedure of Klem and Davisson (47). Stock solutions of IGPS (0.1 mM), PRFAR (120 mM), and glutamine (48 mM) were prepared in a buffer containing 50 mM Tris·HCl, 50 mM KCl, and 1 mM EDTA at pH 8.0. Solutions of PRFAR-bound IGPS [[IGPS] ∼ 1 μM; [PRFAR] ∼ 1 mM (WT) and 11.5 mM (V12A, K19A, V48A, D98A)] were incubated at 30 °C with 0–15 mM Gln for 20 min and then boiled for 4 min and immediately frozen at −80 °C to quench the reaction. To quantitate glutamate production, solutions of GDH (10 mg/mL) and APAD (70 mM) were made in an identical buffer containing 50 mM Tris·HCl, 50 mM KCl, and 1 mM EDTA at pH 8.0. Frozen aliquots of the previously quenched reactions were thawed, and 0.5 mM APAD and 100 μg of GDH were added. The reaction mixtures were incubated at 37 °C for an additional 65 min, and the concentration of APADH, which is formed during the 1:1 conversion of glutamate to 2-oxoglutarate by GDH, was determined by measuring the absorbance of the solution at 363 nm (ε_{363} = 8,900 $M^{-1}\cdot cm^{-1}$). Data were plotted and analyzed with a Michaelis–Menten kinetic model in GraphPad Prism 7.0.

Fluorescence Quenching Titrations. Tryptophan fluorescence emission was monitored at room temperature from 300–400 nm following excitation at 295 nm with 1-nm increments and a 1-s signal averaging time. Samples of IGPS (1–10 μM) were titrated with PRFAR (120 mM stock) until no change was observed in the intensity of λ_{max} (328 nm). Data were analyzed in GraphPad Prism 7.0 and expressed as a percentage of quenched intensity based on the maximum emission of the initial scan (at 0 mM PRFAR).

SI Appendix. *SI Appendix* includes ^{1}H^{15}N-HSQC ligand titration spectra, ^{1}H^{13}C ILV-methyl NMR spectra, raw fluorescence emission scans, tables, and additional histograms of relaxation dispersion parameters.

ACKNOWLEDGMENTS. This work was supported by NIH Grant GM106121 (to J.P.L. and V.S.B.), and K.W.E. acknowledges support from NIH F31 Award GM115223.

1. Monod J, Wyman J, Changeux JP (1965) On the nature of allosteric transitions: A plausible model. *J Mol Biol* 12:88–118.
2. Koshland DE, Jr, Némethy G, Filmer D (1966) Comparison of experimental binding data and theoretical models in proteins containing subunits. *Biochemistry* 5:365–385.
3. Hilser VJ (2010) Biochemistry. An ensemble view of allostery. *Science* 327:653–654.
4. Motlagh HN, Wrabl JO, Li J, Hilser VJ (2014) The ensemble nature of allostery. *Nature* 508:331–339.
5. Nussinov R, Tsai C-J (2015) Allostery without a conformational change? Revisiting the paradigm. *Curr Opin Struct Biol* 30:17–24.
6. Lisi GP, Loria JP (2016) Solution NMR spectroscopy for the study of enzyme allostery. *Chem Rev* 116:6323–6369.
7. Gunasekaran K, Ma B, Nussinov R (2004) Is allostery an intrinsic property of *all* dynamic proteins? *Proteins* 57:433–443.
8. Popovych N, Sun S, Ebright RH, Kalodimos CG (2006) Dynamically driven protein allostery. *Nat Struct Mol Biol* 13:831–838.
9. Petit CM, Zhang J, Sapienza PJ, Fuentes EJ, Lee AL (2009) Hidden dynamic allostery in a PDZ domain. *Proc Natl Acad Sci USA* 106:18249–18254.
10. Boehr DD, Nussinov R, Wright PE (2009) The role of dynamic conformational ensembles in biomolecular recognition. *Nat Chem Biol* 5:789–796.
11. Wand AJ (2001) Dynamic activation of protein function: A view emerging from NMR spectroscopy. *Nat Struct Biol* 8:926–931.
12. Tzeng SR, Kalodimos CG (2011) Protein dynamics and allostery: An NMR view. *Curr Opin Struct Biol* 21:62–67.
13. Aghajanian S, Engel PC (1998) Use of protein engineering to explore subunit interactions in an allosteric enzyme: Construction of inter-subunit hybrids in *Clostridium symbiosum* glutamate dehydrogenase. *Protein Eng* 11:569–575.
14. Lee J, et al. (2008) Surface sites for engineering allosteric control in proteins. *Science* 322:438–442.
15. Nussinov R, Tsai CJ (2013) Allostery in disease and in drug discovery. *Cell* 153:293–305.
16. Velyvis A, Yang YR, Schachman HK, Kay LE (2007) A solution NMR study showing that active site ligands and nucleotides directly perturb the allosteric equilibrium in aspartate transcarbamoylase. *Proc Natl Acad Sci USA* 104:8815–8820.
17. Mazhab-Jafari MT, et al. (2007) Understanding cAMP-dependent allostery by NMR spectroscopy: Comparative analysis of the EPAC1 cAMP-binding domain in its apo and cAMP-bound states. *J Am Chem Soc* 129:14482–14492.
18. Popovych N, Tzeng SR, Tonelli M, Ebright RH, Kalodimos CG (2009) Structural basis for cAMP-mediated allosteric control of the catabolite activator protein. *Proc Natl Acad Sci USA* 106:6927–6932.
19. Selvaratnam R, Akimoto M, VanSchouwen B, Melacini G (2012) cAMP-dependent allostery and dynamics in Epac: An NMR view. *Biochem Soc Trans* 40:219–223.
20. Masterson LR, Cembran A, Shi L, Veglia G (2012) Allostery and binding cooperativity of the catalytic subunit of protein kinase A by NMR spectroscopy and molecular dynamics simulations. *Adv Protein Chem Struct Biol* 87:363–389.
21. Srivastava AK, et al. (2014) Synchronous opening and closing motions are essential for cAMP-dependent protein kinase A signaling. *Structure* 22:1735–1743.
22. Lisi GP, et al. (2016) Dissecting dynamic allosteric pathways using chemically related small-molecule activators. *Structure* 24:1155–1166.
23. Lipchock J, Loria JP (2009) Millisecond dynamics in the allosteric enzyme imidazole glycerol phosphate synthase (IGPS) from *Thermotoga maritima*. *J Biomol NMR* 45: 73–84.
24. Lipchock JM, Loria JP (2010) Nanometer propagation of millisecond motions in V-type allostery. *Structure* 18:1596–1607.
25. Rivalta I, et al. (2012) Allosteric pathways in imidazole glycerol phosphate synthase. *Proc Natl Acad Sci USA* 109:E1428–E1436.
26. Manley G, Rivalta I, Loria JP (2013) Solution NMR and computational methods for understanding protein allostery. *J Phys Chem B* 117:3063–3073.
27. Pervushin K, Riek R, Wider G, Wüthrich K (1997) Attenuated T2 relaxation by mutual cancellation of dipole-dipole coupling and chemical shift anisotropy indicates an avenue to NMR structures of very large biological macromolecules in solution. *Proc Natl Acad Sci USA* 94:12366–12371.
28. Akaike H (1974) A new look at the statistical model identification. *IEEE Trans Automat Contr* 19:716–723.
29. Rivalta I, et al. (2016) Allosteric communication disrupted by a small molecule binding to the imidazole glycerol phosphate synthase protein-protein interface. *Biochemistry* 55:6484–6494.
30. Myers RS, Jensen JR, Deras IL, Smith JL, Davisson VJ (2003) Substrate-induced changes in the ammonia channel for imidazole glycerol phosphate synthase. *Biochemistry* 42: 7013–7022.
31. List F, et al. (2012) Catalysis uncoupling in a glutamine amidotransferase bienzyme by unblocking the glutaminase active site. *Chem Biol* 19:1589–1599.
32. Kim J, et al. (2015) Dysfunctional conformational dynamics of protein kinase A induced by a lethal mutant of phospholamban hinder phosphorylation. *Proc Natl Acad Sci USA* 112:3716–3721.
33. Sapienza PJ, Lee AL (2016) Widespread perturbation of function, structure, and dynamics by a conservative single-atom substitution in thymidylate synthase. *Biochemistry* 55:5702–5713.
34. Tugarinov V, Kay LE (2003) Ile, Leu, and Val methyl assignments of the 723-residue malate synthase G using a new labeling strategy and novel NMR methods. *J Am Chem Soc* 125:13868–13878.
35. Tugarinov V, Kanelis V, Kay LE (2006) Isotope labeling strategies for the study of high-molecular-weight proteins by solution NMR spectroscopy. *Nat Protoc* 1:749–754.
36. Chittur SV, Klem TJ, Shafer CM, Davisson VJ (2001) Mechanism for acivicin inactivation of triad glutamine amidotransferases. *Biochemistry* 40:876–887.
37. Korzhnev DM, Kloiber K, Kanelis V, Tugarinov V, Kay LE (2004) Probing slow dynamics in high molecular weight proteins by methyl-TROSY NMR spectroscopy: Application to a 723-residue enzyme. *J Am Chem Soc* 126:3964–3973.
38. Korzhnev DM, Kloiber K, Kay LE (2004) Multiple-quantum relaxation dispersion NMR spectroscopy probing millisecond time-scale dynamics in proteins: Theory and application. *J Am Chem Soc* 126:7320–7329.
39. Delaglio F, et al. (1995) NMRPipe: A multidimensional spectral processing system based on UNIX pipes. *J Biomol NMR* 6:277–293.
40. Goddard TD, Kneller DG (2008) SPARKY 3 (University of California, San Francisco).
41. d'Auvergne EJ, Gooley PR (2008) Optimisation of NMR dynamic models I. Minimisation algorithms and their performance within the model-free and Brownian rotational diffusion spaces. *J Biomol NMR* 40:107–119.
42. d'Auvergne EJ, Gooley PR (2008) Optimisation of NMR dynamic models II. A new methodology for the dual optimisation of the model-free parameters and the Brownian rotational diffusion tensor. *J Biomol NMR* 40:121–133.
43. Bieri M, d'Auvergne EJ, Gooley PR (2011) relaxGUI: A new software for fast and simple NMR relaxation data analysis and calculation of ps-ns and μs motion of proteins. *J Biomol NMR* 50:147–155.
44. Morin S, et al. (2014) relax: The analysis of biomolecular kinetics and thermodynamics using NMR relaxation dispersion data. *Bioinformatics* 30:2219–2220.
45. Devore JL (2000) *Probability and Statistics for Engineering and the Sciences* (Brooks/Cole Publishing, Pacific Grove, CA).
46. Motulsky H, Christopoulos A (2004) *Fitting Models to Biological Data Using Linear and Non-Linear Regression: A Practical Guide to Curve Fitting* (Oxford Univ Press, New York).
47. Klem TJ, Davisson VJ (1993) Imidazole glycerol phosphate synthase: The glutamine amidotransferase in histidine biosynthesis. *Biochemistry* 32:5177–5186.
48. Schrödinger LLC (2016) The Pymol Molecular Graphics System, Version 1.8 (Schrödinger, LLC, New York).
49. Grzesiek S, Stahl SJ, Wingfield PT, Bax A (1996) The CD4 determinant for downregulation by HIV-1 Nef directly binds to Nef. Mapping of the Nef binding surface by NMR. *Biochemistry* 35:10256–10261.
50. Scott DW (1979) On optimal and data-based histograms. *Biometrika* 66:605–610.
51. Wintjens R, et al. (2001) 1H NMR study on the binding of Pin1 Trp-Trp domain with phosphothreonine peptides. *J Biol Chem* 276:25150–25156.